Journal of the Meteorological Society of Japan

EARLY ONLINE RELEASE

The DOI for this manuscript is
DOI:10.2151/jmsj.2021-021
J-STAGE Advance published date: January th, 2021

A New Graphical Method to Diagnose the Impacts of Model Changes on Climate Sensitivity

Shipra JAIN

Centre for Atmospheric Sciences, Indian Institute of Technology Delhi, India
Department of Geophysics, Kyoto University, Kyoto, Japan
School of Geosciences, University of Edinburgh, Edinburgh, United Kingdom

Rattana CHHIN

Department of Geophysics, Kyoto University, Kyoto, Japan
Research and Innovation Center, Institute of Technology of Cambodia, Cambodia

Ruth M. DOHERTY

School of Geosciences, University of Edinburgh, Edinburgh, United Kingdom

Saroj K. MISHRA

Centre for Atmospheric Sciences, Indian Institute of Technology Delhi, India

and

Shigeo YODEN

Department of Geophysics, Kyoto University, Kyoto, Japan
Institute for Liberal Arts and Sciences, Kyoto University, Kyoto, Japan

November 16, 2019
April 25, 2020, revised
October 4, 2020, revised

---

1) Corresponding author: Shigeo Yoden, Institute for Liberal Arts and Sciences, Kyoto University, Kyoto 606-8501 JAPAN.
Email: yoden.shigeo.53r@st.kyoto-u.ac.jp
Tel: +81-75-753-6565
Fax: +81-75-753-7851

Abstract

Equilibrium climate sensitivity (ECS) is defined as the change in global-mean surface air temperature due to the doubling or quadrupling of CO_2 in a climate model simulation. This metric is used to determine the uncertainty in future climate projections, and therefore the impact of model changes on ECS is of large interest to the climate modeling community. In this paper, we propose a new graphical method, which is an extension of the Gregory's linear regression method, to represent the impact of model changes on ECS, climate forcing and climate feedbacks in a single diagram. Using this visualization method, one can quantify (a) whether the model- or process-change amplifies, reduces, or has no impact on global warming, (b) the percentage changes in ECS, climate forcing and climate feedbacks, and (c) the uncertainties in the estimated changes. We demonstrate this method using an example of climate sensitivity simulations with and without interactive chemistry. This method can be useful for multi-model assessments where the response of multiple models for the same model experiment (e.g., usage of interactive chemistry as compared to the prescribed chemistry as shown here) can be assessed simultaneously, which is otherwise difficult to compare and comprehend. We also demonstrate how this method can be used to examine the spread in ECS, climate forcing and climate feedbacks with respect to the multi-model mean (or one benchmark model) for multi-model frameworks like Coupled Model Intercomparison Project Phase 5 or for different ensemble members in a large ensemble of simulations carried out using a

single model.

Keywords new graphical method, climate sensitivity, interactive chemistry, climate forcing and climate feedbacks, multi-model assessments.

1. Introduction

The Earth's climate is sensitive to the concentrations of greenhouse gases (GHGs) in the atmosphere. The concentrations of GHGs have a large impact on radiative forcing and surface climate change. One widely used metric to estimate this impact is Equilibrium Climate Sensitivity (ECS). ECS, which is defined as the response of global and annual mean surface air temperatures to a change in GHG concentrations, can be calculated using an idealized long-period climate simulation in which atmospheric CO_2 concentration is instantaneously doubled ($2\times CO_2$) or quadrupled ($4\times CO_2$) from the pre-industrial (PI) level. Climate sensitivity is also used as a measure of uncertainty for the assessment of future projections in similarly forced General Circulation Models (GCMs) or Earth System Models (ESMs). A wide range of climate sensitivity across models would imply a lower confidence in future projections, and therefore continuous efforts are being made to determine and understand the factors on which the climate sensitivity depends in models.

Recent research shows using interactive chemistry in place of prescribed values, as done in Coupled Model Intercomparison Project Phase 5 (CMIP5), can impact surface climate and estimates of ECS in climate models (e.g., Chiodo et al. 2016; Dietmuller et al. 2014; Marsh et al. 2016; Muthers et al. 2014; Nowack et al. 2015, 2017, 2018). Nowack et al. (2015), using the UK Met Office chemistry-climate model, showed that the global mean surface warming is reduced by ~1 K (~20%) when the model computes the chemistry processes interactively in place of using prescribed values at PI levels. In contrast to this,

Marsh et al. (2016) showed no large impacts of interactive chemistry on the climate sensitivity in the Community Earth System Model - Whole Atmosphere Community Climate Model (CESM1-WACCM).

To evaluate the response of surface climate to the imposed forcing (doubling or quadrupling of CO_2), these studies utilized the following linear energy balance equation introduced by Gregory et al. (2004) and used by others (Aldrin et al. 2012; Andrew et al. 2012; Annan and Hargreaves 2006; Dessler and Forster 2018; Lewis and Curry 2015; Otto et al. 2013; Skeie et al. 2014):

$$N(t) = F + \alpha \Delta T(t), \quad (1)$$

where t is time (annual-mean), N (t) is the net radiative flux (Wm^{-2}) at the top of the atmosphere (TOA), F is the imposed forcing (Wm^{-2}), α is the climate feedback parameter ($Wm^{-2}\ K^{-1}$), and ΔT (t) is the global mean surface air temperature change (K). Equation (1) is linear and therefore F can be estimated by the y-axis intercept and α by the slope of the line of best fit from the scatter plot of ΔT (t) versus N (t). ECS is defined as the global-mean equilibrium surface-air-temperature change ΔT in response to abrupt $2\times CO_2$ or $4\times CO_2$ experiments (Andrews et al. 2012) under the limit of time t tending to very large values (generally hundreds of years for atmosphere-ocean coupled GCMs). It is a convenient metric of quantifying the joint effect of climate forcing and climate feedbacks under the implicit assumption of N approaching zero. ECS is given as $-F/\alpha$ in a $2\times CO_2$ experiment, whereas it is $-F/(2\alpha)$ in a $4\times CO_2$ experiment.

Though the information that is provided in the climate sensitivity studies is of extreme importance for future climate change assessments, the results presented in these papers can be challenging to comprehend unless accompanied with detailed textual description. These studies also emphasize the need for multi-model assessments in which each model's response to the interactive chemistry should be compared with its prescribed chemistry simulation, and also with the results of other models for the same experiment. However, in that case, the intercomparison of the myriad of results will be complex. To overcome this, we propose a new graphical method in which information that is typically presented in the form of text and tables can be summarized and collated in one single diagram.

One of the applications of this method is for multi-model assessments in which the impact of model- or process-change on ECS, climate forcing and climate feedbacks can be simultaneously diagnosed for multiple models. Using the proposed method, each model can be represented by its own marker with standard error intervals in a single diagram, which simplifies the intercomparison of multiple models for the same experimental framework (e.g., using interactive chemistry in place of prescribed values in each model). In this paper, we demonstrate this method using the example of climate sensitivity simulations with interactive and prescribed chemistry, carried out using Japan Meteorological Agency - Meteorological Research Institute (JMA-MRI) Earth System and coupled atmosphere-ocean models. We also show how this method can be used to estimate the spread in ECS, climate forcing and climate feedbacks for multiple models with respect to the multi-model mean (or a benchmark

model), using CMIP5/6 or other data. This method can also be used to estimate the spread or change in these three parameters for a large ensemble of simulations done by using a single model.

Section 2 describes the method and data that are used in this paper. Section 3 demonstrates the application of this graphical method for three different examples, and Section 4 summarizes the key highlights of this paper.

2. Description of the Method and Data

2.1 Linear regression to estimate forcing and feedbacks

We first present a general form of this method for two sets of climate sensitivity simulations with (i) a control (*ctrl*) simulation and (ii) an experiment (*expt*) simulation, which is same as *ctrl* but with a model process or a parameter value changed to investigate its impact on climate sensitivity.

For a simulation x (= *ctrl* or *expt*), the change in global-mean surface air temperature in the abrupt $4\times CO_2$ experiment (denoted by 4C in subscript) with respect to the PI climatology is given as:

$$\Delta T_x(t) = T_{4C,x}(t) - \overline{T}_{PI,x}, \quad (2)$$

where $T_{4C,x}(t)$ is the global-mean surface air temperature (K) in the 4C experiment, and $\overline{\mathbf{T}}_{PI,x}$ is the climatological (time-mean) temperature for the PI simulation. Similarly, a change in the net radiation flux is given as:

$$\Delta N_x(t) = N_{4C,x}(t) - \bar{N}_{PI,x} . \quad (3)$$

Note that Eq. (1) is for the scenario where the model is initially in an equilibrium state such that the net radiative imbalance at the TOA is zero in the PI simulation. However, if the model is in an initial non-stationary state (i.e., the value of N in the PI simulation is non-zero), one should remove the radiative imbalance noted in the PI simulation from the 4C simulation. In this case, the variable N should be replaced by ΔN to account for the radiative imbalance, if there is any, in the initial state. Equation (1) can, therefore, be re-written as:

$$\Delta N_x(t) = F_x + \alpha_x \Delta T_x(t) , \quad (4)$$

where $\Delta N_x(t)$ and $\Delta T_x(t)$ can be regressed for *ctrl* and *expt* simulations separately for the full simulation period after the abrupt quadrupling of the CO_2, and the values for the climate feedback parameter α_x (x = *ctrl* or *expt*) and the imposed forcing F_x are estimated using the lines of best fit.

2.2 Impact analysis

As Eq. (4) can be re-written as $\Delta T_x(t) = (\Delta N_x(t) - F_x) / \alpha_x$, the ratio of the two $\Delta T_x(t)$ for *ctrl* and *expt* is given by:

$$\frac{\mathbf{\Delta T_{expt}(t)}}{\mathbf{\Delta T_{ctrl}(t)}} = \frac{\mathbf{\alpha_{ctrl}}}{\mathbf{\alpha_{expt}}} \times \frac{\mathbf{\Delta N_{expt}(t) - F_{expt}}}{\mathbf{\Delta N_{ctrl}(t) - F_{ctrl}}} = \frac{\mathbf{R_F(t)}}{\mathbf{R_\alpha}} , \quad (5)$$

where R_α is the ratio of the climate feedback parameter α_x for *ctrl* and *expt*, and $R_F(t)$ is the ratio of the difference between the net radiation flux at the TOA and the imposed forcing, $\Delta N_x(t) - F_x$, for *ctrl* and *expt*. From this relationship, the impact of *expt* on the global-mean

surface air temperature change in the *ctrl* simulation is given by:

$$\Delta T_{expt}(t) - \Delta T_{ctrl}(t) = \left(\frac{R_F(t)}{R_\alpha} - 1\right) \times \Delta T_{ctrl}(t) \,. \qquad (6)$$

Note that Eq. (6) can be used to determine the time evolution of the change in the global-mean surface air temperature. To determine the equilibrium response of the surface air temperature, i.e., ECS, we replace all time-varying components in Eq. (6) by their respective climatological means:

$$\overline{\Delta T}_{expt} - \overline{\Delta T}_{ctrl} = \left(\frac{\bar{R}_F}{R_\alpha} - 1\right) \times \overline{\Delta T}_{ctrl} \,, \qquad (7)$$

where $\bar{R}_F = (\overline{\Delta N}_{expt} - F_{expt}) / (\overline{\Delta N}_{ctrl} - F_{ctrl})$, and $\overline{\Delta N}_x$ must be calculated for the period when the model is in equilibrium or quasi-equilibrium state, excluding the initial transient response to the abrupt quadrupling of CO_2. Note that the % change in ECS in the *expt* simulation with respect to *ctrl* simulation is given as $[(\bar{R}_F / R_\alpha) - 1] \times 100$.

Equation (7) leads to five possible scenarios (Case 0 to IV) as follows:

Case 0: $\bar{R}_F = R_\alpha$ and ΔT_{ctrl} = any value,

the impact of the experiment on the global-mean surface air temperature, i.e., ECS, is zero.

Case I: $\bar{R}_F > R_\alpha$ and $\Delta T_{ctrl} > 0$,

represents the case of global warming as $\Delta T_{ctrl} > 0$, and the warming is amplified.

Case II: $\bar{R}_F > R_\alpha$ and $\Delta T_{ctrl} < 0$,

represents the case of global cooling as $\Delta T_{ctrl} < 0$, and the cooling is amplified.

Case III: $\bar{R}_F < R_\alpha$ and $\Delta T_{ctrl} > 0$,

represents the case of global warming as $\Delta T_{ctrl} > 0$, and the warming is reduced.

Case IV: $\bar{R}_F < R_\alpha$ and $\Delta T_{ctrl} < 0$,

represents the case of global cooling as $\Delta T_{ctrl} < 0$, and the cooling is reduced.

2.3 Uncertainty in feedback parameter, forcing, and their ratios

Given that the relationship between ΔN_x (t) and ΔT_x (t) is not entirely linear in a model simulation, there will be associated uncertainties in α_x and F_x that are estimated using the linear regression. The possible values for α_x are given by $\alpha_x \pm E_{\alpha,x}$ and F_x by $F_x \pm E_{F,x}$, where $E_{\alpha,x}$ and $E_{F,x}$ are the uncertainties in α_x and F_x, respectively. The uncertainties (or the standard errors), E_α and E_F, are given as follows (e.g., Montgomery et al., 2012):

$$E_{\alpha,x}^2 = \frac{\sigma_x^2 \, I}{I\sum_{i=1}^{I}(\Delta T_{x,i})^2 - (\sum_{i=1}^{I}\Delta T_{x,i})^2} \quad , \tag{8}$$

$$E_{F,x}^2 = \frac{\sigma_x^2 \sum_{i=1}^{I}(\Delta T_{x,i})^2}{I\sum_{i=1}^{I}(\Delta T_{x,i})^2 - (\sum_{i=1}^{I}\Delta T_{x,i})^2} \quad , \tag{9}$$

where i is a sequential integer for each year, and I is the total number of years used for the linear regression, and σ_x is given as:

$$\sigma_x^2 = \frac{\sum_{i=1}^{I}(\Delta N_{x,i} - F_x - \alpha_x \Delta T_{x,i})^2}{I-2} \quad . \tag{10}$$

The uncertainties $E_{\alpha,x}$ and $E_{F,x}$ are obtained for both *ctrl* and *expt* simulations. The magnitudes of uncertainty for the ratios R_α and R_F are also obtained using the law of propagation of errors (e.g., Bohm and Zech, 2014):

$$E_{R_\alpha} = R_\alpha \sqrt{\left(\frac{E_{\alpha,expt}}{\alpha_{expt}}\right)^2 + \left(\frac{E_{\alpha,ctrl}}{\alpha_{ctrl}}\right)^2} \quad , \tag{11}$$

$$E_{R_F} = R_F \sqrt{\left(\frac{E_{H,expt}}{H_{expt}}\right)^2 + \left(\frac{E_{H,ctrl}}{H_{ctrl}}\right)^2} \quad , \tag{12}$$

$$H_x = \overline{\Delta N}_x - F_x \ , \quad (13)$$

$$E_{H,x} = \sqrt{E^2_{\overline{\Delta N},x} + E^2_{F,x}} \ , \quad (14)$$

where $E_{\overline{\Delta N},x}$ is the standard error in $\overline{\Delta N}_x$ and given as:

$$E_{\overline{\Delta N},x} = \frac{\sigma_{\Delta N,x}}{\sqrt{J}} \ , \quad (15)$$

where J is the number of model years used to calculate $\overline{\Delta N}_x$ and $\sigma_{\Delta N,x}$ is the standard deviation in ΔN_x (t) for the J years.

It is also noted that each year in ΔT (t) and ΔN (t) time series is not independent (Gregory et al. 2004), which would lead to the underestimation of the errors calculated above. The appropriate statistical confidence intervals can be obtained by replacing the total number of model years used for the error estimation (i.e., I or J) by the effective number of years estimated after the consideration of time-lag correlation (e.g., Naito and Yoden 2005) or by using the boot-strapping method as used by Andrews et al. (2012).

2.4 Model simulations and data

We demonstrate the application of this method using two sets of simulations; (i) PI and 4C simulations with prescribed chemistry (FIXED, instead of *ctrl* above) and (ii) PI and 4C simulations with interactive chemistry (ACTIVE, instead of *expt* above). For the experiments with the prescribed chemistry (PI FIXED and 4C FIXED), the MRI atmosphere-ocean-aerosol GCM, CGCM3 (Yukimoto et al., 2012) was used. On the other hand, the simulations with interactive chemistry (PI ACTIVE and 4C ACTIVE) were carried out using MRI ESM1

(Earth System Model version 1, Adachi et al. 2013; Yukimoto et al. 2011).

The MRI ESM1 and CGCM3 models employed in this study are the same as those used by Noda et al. (2017, 2018) for similar PI FIXED and PI ACTIVE experiments for paleoclimates (Mid-Holocene and the Last Glacial Maximum, respectively). The carbon cycle processes were deactivated in the ESM1 simulations carried out here (for both PI and 4C), although the MRI-ESM1 simulations in CMIP5 employed the carbon cycle processes. Both MRI ESM1 and CGCM3 have the same components except for the chemical component, which includes 90 chemical species with 172 gas-phase reactions, 59 photolysis reactions, and 16 heterogeneous reactions, and also includes improved grid-scale transport with a semi-Lagrangian scheme (Yukimoto et al. 2011). For the FIXED PI and 4C simulations, the concentrations of the chemical species are prescribed at 1850 level. The stratosphere includes seasonal and latitude-height variations of the chemical species whereas the troposphere includes seasonal and 3-D variations of the species. The ozone values are taken from Atmospheric Chemistry and Climate / Stratosphere-troposphere Processes And their Role in Climate (ACC/SPARC) database (https://climatedataguide.ucar.edu/climate-data/stratospheric-tropospheric-ozone-accsparc-atmospheric-chemistry-and-climate, last access 3 October 2020). The concentrations of other GHGs and anthropogenic aerosols or their pre-cursors at 1850 level are taken from the Representative Concentration Pathways (RCP) database (http://www.iiasa.ac.at/web-apps/tnt/RcpDb, last access: 3 October 2020). More details on

the prescribed chemical species are provided in Yukimoto et al. (2012). For ACTIVE PI and 4C simulations, the model had the initial chemical concentrations at 1850 level which were taken from the “esmControl” run in CMIP5, which is the same as the ACTIVE PI simulation here.

For PI simulations, we use the same datasets of 100 years as obtained by Noda et al. (2017) for both FIXED and ACTIVE simulations. There is no significant climate drift noted in the 100-year PI simulation. For 4C simulations (both FIXED and ACTIVE), the model was started using the restart files of corresponding PI runs, and run for 110 years in total, with the CO_2 quadrupled abruptly after 10 years. The horizontal resolution of the model was a triangular truncation at the maximum wavenumber 42 (T42), corresponding to a grid resolution of ~2.8 degrees across longitude and latitude. The model had 68 vertical layers (L68) extending from the surface to the mesopause, 0.01 hPa (Deushi and Shibata 2011). The treatment of water vapor feedback was similar to that described in Noda et al. (2018). More details on the model setup can be found in Noda et al. (2017, 2018).

The output data from 16 CMIP5 models were also utilized to demonstrate the application of this method for multi-model frameworks (Subsection 3.3). The CMIP5 data were obtained from Earth System Grid Federation (ESGF) website (https://esgf-node.llnl.gov/search/esgf-llnl/, last access 3 October 2020).

3. Results

3.1 Demonstration of the method — Impact of interactive chemistry

To demonstrate this graphical method, we use the two sets of climate sensitivity simulation data generated from the MRI models, i.e., ACTIVE and FIXED for PI and 4C simulations as described in the previous section. Figure 1 (a) shows the time series of ΔT_x (t) as given by Eq. (2) for ACTIVE (blue) and FIXED (red) simulations. The vertical dotted line marks the time t = 0 when CO_2 concentration is quadrupled and the time before t = 0 corresponds to the PI condition. The response of the global-mean surface air temperature anomalies to the abrupt 4×CO_2 is evident in the initial few decades, and the temperature changes asymptote to a similar value for both ACTIVE and FIXED simulations for around the last 50 years.

Fig. 1

Figure 1 (b) shows ΔN_x (t) vs ΔT_x (t) for the last 100 years of ACTIVE and FIXED simulations. The initial 10 years of the 110 years simulation are discarded as they correspond to the period before the quadrupling of CO_2 concentration. Figure 1 (b) confirms the almost linear relationship between ΔN_x (t) and ΔT_x (t), and α_x and F_x are estimated by the slope and intercept of the lines of best fit (solid blue and red lines, respectively). Note that we use the data for the full 4×CO_2 period (i.e., 100 years) to determine the coefficients α_x and F_x using the linear regression. The ratio R_α is obtained using α_x, and the ratio $\overline{R}_F$ is obtained from $\overline{\Delta N_x}$ and F_x as defined in Eq. (7). To calculate the climatological mean of ΔN_x, i.e. $\overline{\Delta N_x}$, we use data for the last 50 years of the simulation period, when the model is in quasi-equilibrium state. The values of $\overline{\Delta N_x}$ are shown by horizontal dotted lines with the

Table 1

corresponding color in Fig. 1 (b). The standard errors in α_x are estimated using Eqs. (8) and (10), and those in F_x are estimated using Eqs. (9) and (10), with i=1 to 100 (=I). The errors in $\overline{\Delta N_x}$ are calculated using Eq. (15), with J = 50. The errors in R_α and $\overline{R}_F$ are estimated using Eqs. (11)-(15). The values of all quantities and their corresponding errors are provided in Table 1.

Figure 2 shows the obtained value of R_α and $\overline{R}_F$ (black dot) with its standard errors (horizontal and vertical bars, as described in Subsection 2.3) on R_α – $\overline{R}_F$ plane. Figure 2 is our proposed new graphic method to visualize the impact of model changes on ECS, climate forcing, and climate feedbacks. The abscissa, R_α, represents the ratio of the climate feedback parameter. The unity value of R_α represents no change in the climate feedback parameter α_x, and every 0.1 increase (or decrease) in the magnitude of R_α corresponds to the 10% increase (or decrease) in feedback strength in ACTIVE simulation as compared to FIXED simulation. Similarly, the unity value on the ordinate, $\overline{R}_F$ = 1, represents no change in the difference between radiative flux imbalance and forcing ($\overline{\Delta N_x}$ – F_x).

Fig. 2

The % change in ECS in ACTIVE simulation with respect to FIXED simulation is given by [($\overline{R}_F$/ R_α) – 1] × 100. The thick black dashed line represents Case 0 as described in Subsection 2.2 with $\overline{R}_F$ = R_α, and therefore corresponds to the case of no impact of the experiment on the global mean surface air temperature, or ECS. This line is referred to as the no-impact line. Any point lying above this no-impact line corresponds to Case I (as ΔT_{ctrl} > 0) with $\overline{R}_F$ > R_α, and thus represents the amplification of global warming in the ACTIVE

as compared to the FIXED simulation. On the other hand, any point lying below the no-impact line corresponds to Case III with $\overline{R}_F$ < R_α, representing the reduction of global warming in the ACTIVE as compared to FIXED simulation. Four red (blue) dashed lines in the plot show consecutive 10% increases (decreases) in the values of ECS up to ±40%: $\overline{R}_F = (1 \pm \frac{a\,\%}{100\%})\ R_\alpha$, (a=10, 20, 30 and 40).

In the present example, R_α is ~1.08±0.04, which implies the climate feedback parameter α_x is increased by ~8% in ACTIVE as compared to FIXED simulation with the standard error of ± 4%. Similarly, $\overline{R}_F$ is ~1.10±0.04, which means the difference between radiative flux imbalance and forcing ($\overline{\Delta N}_x - F_x$) is also increased by ~10% with a standard error of 4%. As a result, the ratio $\overline{R}_F/R_\alpha$ remains close to 1 with only a 1.5% increase in ECS. It can be concluded from Fig. 2 that the impact of interactive chemistry on ECS is small in the MRI climate models. The scatter in the linear fit for ΔN_x (t) vs ΔT_x (t) is quite small for the MRI models (Fig. 1b), and therefore the uncertainties are also small. We have data only from MRI models for this demonstration and therefore there is only one symbol in Fig. 2. However, if the multi-model outputs are available for the same experimental framework (e.g., for interactive and prescribed chemistry), then each model can be plotted by its own symbol in this diagram, and intercomparison of ECS, climate forcing and climate feedbacks for the multiple models is straightforward.

3.2 Application to individual radiative components

According to the linear climate feedback theory, the net global climate feedback is the linear sum of longwave (LW) and shortwave (SW) contributions for each clear-sky (CS) and cloud radiative effect (CRE) component, as described in the Methods section of Nowack et al. (2015). The net radiative imbalance at the TOA due to all radiative components is the linear sum of the imbalance caused by the four individual components (CS-LW, CS-SW, CRE-LW, and CRE-SW).

The corresponding values of ΔN (t) and ΔT (t) are almost linearly related for the individual radiative components in each FIXED and ACTIVE simulation as shown in Fig. 3 (a) and (b). The values of all metrics for the individual radiative components are obtained by estimating Gregory linear relations for CS and CRE components separately and given in Table 1. The CS radiative feedback, which is given by the slope of the line of best fit, is much larger in magnitude than the CRE feedback for both LW and SW components. Furthermore, the feedback for LW and SW components are opposite in sign with larger magnitudes for LW for both the CS and CRE components (see Table 1 for the estimated values). This indicates that the longwave feedbacks in the atmosphere are partially offset by the corresponding shortwave feedbacks.

Fig. 3

The values of R_α and $\overline{R}_F$ (and their uncertainties) for individual and all radiative components are plotted in Fig. 3 (c). The CRE-SW (CRE-LW) component shows a large reduction of ~40.0% (~19.7%) in the climate feedback with a relatively smaller reduction of ~34.3% (~16.7%) in the climate forcing, thus indicating a net amplification of the global

warming by ~9.4% (~3.7%) in ACTIVE as compared to FIXED simulation. Both CS-LW and CS-SW components show small changes with the same tendency in the feedback and forcing (~2-4% increase and ~3-4% decrease, respectively); thus the ratios R_α and $\overline{R}_F$ for these components remain close to one. The uncertainties in ratios R_α and $\overline{R}_F$ are also large for CRE components as compared to CS components, which is also confirmed by Fig. 3 (a) and (b) that show larger scatter in CRE components as compared to the CS components.

The ACTIVE simulation leads to slight amplification of global warming by ~1.5% as compared to FIXED for all radiative components (black circle), as described in Subsection 3.1. The individual radiative components, CS-LW and CS-SW components lie near the no-impact line and show slight amplification of global warming by about ~1%. The CRE-LW and CRE-SW components show amplification of global warming by about ~4% and 9%, respectively (the bottom row in Table 1). It is also important to mention here that each radiation component is regressed against the same ΔT, and ideally, the impact of individual components on temperatures should be the same and close to the impact noted for the all-radiation component. Here, however, R_α and $\overline{R}_F$ for CRE have a large impact and uncertainty as compared to the all-radiation component. The large uncertainties in the CRE component arise due to the large scatter in the linear fit and smaller values of climate feedback and climate forcing as compared to the CS component as shown in Fig. 3 (a) and 3(b) (see also Eqs. (11) and (12)).

3.3 Application to multiple CMIP5 models

In the previous subsections, we showed the impact of interactive chemistry on ECS, climate forcing and climate feedbacks for the JMA MRI climate models as shown in Figs. 2 and 3(c). Results for other models with the same experimental framework can also be included in this diagram, to compare the outputs of multiple models. Note that in this case, the impact of chemistry is examined by comparing ACTIVE (*expt*) simulation for each model with respect to its own FIXED (*ctrl*) simulation.

Here we demonstrate to use this method to visualize the spread in ECS, climate forcing, and climate feedbacks across multiple CMIP5 models. In this case, *ctrl* simulation can be replaced by the multi-model mean (MMM) and each model can be used as an *expt* simulation, in order to examine the relative difference of ECS, climate forcing and climate feedbacks for each model from the MMM. Figure 4 shows the relative difference of 18 models (16 CMIP5 models and two MRI models used above) from the MMM ($\overline{R}_F = R_\alpha = 1$), plotted with their own symbols as listed.

Fig. 4

The CMIP5 models show a large spread in ECS varying from around – 38% to 35% with respect to the MMM (see Table 2 for the parameter values and standard errors of each model). In total 10 models show more global warming than the MMM (above the black dashed line), whereas the rest of the models show less warming (below the black dashed line) as compared to the MMM. The climate forcing shows a large spread from around – 43% to 39% if compared with the MMM (see $\overline{R}_F$ of the 6th column in Table 2). Similarly, the

Table 2

climate feedback (α) also shows a larger spread from – 46% to 57% with respect to the MMM (the 5th column in Table 2).

The MIROC-ESM model shows the largest warming of ~35% more than the MMM (Case I), which is mainly due to the difference in climate feedback (~25% less than the MMM) whereas the forcing is almost the same as the MMM. Similarly, the INM-CM4 model shows a small difference in the forcing (~2% less than the MMM) whereas the feedback is ~57% more than the MMM, leading to ~38% lower ECS than the MMM (Case III). The CSIRO-Mk3.6.0 model shows the largest reduction in forcing and feedbacks (~ - 43% and ~ - 47%, respectively), but since the changes in both forcing and feedback are comparable, the net impact on ECS remains small (~6%).

It is interesting to note that different models from the same modeling center also show different variations in ECS, climate forcing, and climate feedbacks. For instance, the MIROC5 and MIROC-ESM models are quite different if compared to the pair of MRI models (CGCM3 and ESM1). The MIROC5 model shows ~10% less warming as compared to the MMM, whereas the MIROC-ESM model shows ~35% more warming than the MMM. The forcing for MIROC-ESM is close to the MMM but the feedback is relatively smaller (~ - 25%), whereas, for MIROC5, the feedback and forcing are ~55% and 39% larger, respectively.

Similar to the intermodel comparison with respect to the MMM presented above, one can also compare the outputs of other models with respect to one benchmark model. In such a case, *ctrl* can be replaced by the benchmark model and each model that is being compared

can be represented by *expt*. It is also possible to examine the spread in ECS, climate forcing and climate feedbacks for different ensemble members in a large ensemble of simulations carried out using a single model (e.g., Dessler et al. 2018), with the ensemble mean as *ctrl* and individual members as *expt*.

4. Concluding Remarks

We proposed a new graphical method that provides a concise summary of the impact of model- or process-change on ECS, climate forcing, and climate feedbacks. The method is based on the linear regression method that was introduced by Gregory et al. (2004). Using this method, one can quantify (a) whether the model- or process-change amplifies, reduces, or has no impact on the global warming, (b) the percentage changes in ECS, climate forcing, and climate feedbacks, and (c) the uncertainties in the estimated changes. Using this graph, the outputs of multiple models for the same experimental framework (e.g., usage of interactive chemistry as compared to the prescribed one) can be collated and visualized in one single diagram, which is otherwise difficult to compare and comprehend.

We demonstrated this method using an example of climate sensitivity simulations with and without interactive chemistry with Japan Meteorological Agency – Meteorological Research Institute (JMA-MRI) climate models. An application of this method for four individual radiative components (clear-sky and cloud radiative effects for longwave and shortwave components) was also described, after confirming the appropriateness of the

linear fittings of Gregory's regression. We also presented the application of this method to visualize and quantify the spread in ECS, climate forcing and climate feedbacks for individual models with respect to the multi-model mean in multiple model frameworks like CMIP5 (Taylor et al. 2012), CMIP6 (Eyring et al. 2016), GeoMIP (Kravitz et al. 2011), nonlinMIP (Good et al. 2016), and others. Furthermore, it could be used to determine the differences in these three parameters for multiple models against any benchmark model instead of the multi-model mean or to estimate the spread or change in the three parameters for a large ensemble of simulations done by using a single model (e.g., Dessler et al. 2018).

It is also important to remark here that this method is based on Gregory's linear regression and the uncertainties (or standard errors) in climate forcing and climate feedbacks is calculated under the approximation that the relationship between the net radiative imbalance, ΔN (t), and the global mean surface air temperature change, ΔT (t), is linear. Nonlinear response of ΔT to ΔN, if any, will be included in the uncertainty estimates given in Subsection 2.3. In this paper, we described the graphical method and demonstrated its application using an example of climate sensitivity simulations for instantaneously quadrupled CO_2 with and without interactive chemistry. More detailed findings on the impact of using interactive chemistry on the surface and other atmospheric variables in the MRI climate models will be provided in a separate paper.

Acknowledgments

The authors acknowledge Dr. Satoshi Noda and colleagues of the JMA MRI for providing the simulation data used in this paper. The CMIP5 data were obtained from the ESGF website. The authors are also thankful to Professor Jonathan M. Gregory for the personal discussion provided in Subsection 2.1. This work is partially supported by JSPS KAKENHI Grant Numbers JP15H05816 and JP17H01159, JSPS Core-to-Core program B (Asia-Africa Science Platforms), JSPS & DG-RSTHE Joint Research Program, and DST Centre of Excellence in Climate Modeling. This work and its contributors (SJ and RMD) were partially supported by the UK-China Research & Innovation Partnership Fund through the Met Office Climate Science for Service Partnership (CSSP) China as part of the Newton Fund. The authors declare no financial conflict of interests.

References

Adachi, Y., S. Yukimoto, M. Deushi, A. Obata, H. Nakano, T.Y., Tanaka, M. Hosaka, T. Sakami, H. Yoshimura, M. Hirabara, and E. Shindo, 2013: Basic performance of a new earth system model of the Meteorological Research Institute (MRI-ESM1). *Pap. Meteorol. Geophys.*, **64**, 1-19.

Aldrin, M., M. Holden, P. Guttorp, R.B., Skeie, G., Myhre, and T.K. Berntsen, 2012: Bayesian estimation of climate sensitivity based on a simple climate model fitted to observations of hemispheric temperatures and global ocean heat content. *Environmetrics*, **23(3)**, 253-271, doi:10.1002/env.2140.

458 Andrews, T., J.M. Gregory, M.J. Webb, and K.E. Taylor, 2012: Forcing, feedbacks and
459 climate sensitivity in CMIP5 coupled atmosphere ocean climate models. *Geophys. Res.*
460 *Lett.*, **39**, L09712, doi:10.1029/2012GL051607.
461 Annan, J.D., and J.C. Hargreaves, 2006: Using multiple observationally-based constraints
462 to estimate climate sensitivity. *Geophys. Res. Lett.*, **33**, L06704,
463 doi:10.1029/2005GL025259.
464 Bohm, G., and G. Zech, 2014: *Introduction to statistics and data analysis for physicists.*
465 *Second Revised Edition*. Hamburg: DESY, 469pp, doi:10.3204/DESY-BOOK/statistics.
466 Chiodo, G., and L. Polvani, 2016: Reduction of climate sensitivity to solar forcing due to
467 stratospheric ozone feedback. *J. Climate*, **29**, 4651-4663.
468 Dessler, A.E., and P.M. Forster, 2018: An estimate of equilibrium climate sensitivity from
469 interannual variability. *J. Geophys. Res.*, **123**, 8634-8645,
470 https://doi.org/10.1029/2018JD028481.
471 Dessler, A.E., T. Mauritsen, and B. Stevens, 2018: The influence of internal variability on
472 Earth's energy balance framework and implications for estimating climate sensitivity.
473 *Atmos. Chem. Phys.*, **18**, 5147-5155, https://doi.org/10.5194/acp-18-5147-2018.
474 Deushi, M. and K. Shibata, 2011: Impacts of increases in greenhouse gases and ozone
475 recovery on lower stratospheric circulation and the age of air: Chemistry‐climate model
476 simulations up to 21Geophys*Geophys. Res. Atmospheres*, **116(D7)**, D07107,
477 doi:10.1029/2010JD015024.

Dietmüller, S., M. Ponater, and R. Sausen, 2014: Interactive ozone induces a negative feedback in CO2-driven climate change simulations. *J. Geophys. Res. Atmospheres*, **119.4**, 1796-1805.

Eyring, V., S. Bony, G.A. Meehl, C.A. Senior, B. Stevens, R.J. Stouffer, and K.E. Taylor, 2016: Overview of the Coupled Model Intercomparison Project Phase 6 (CMIP6) experimental design and organization. *Geosci. Model Dev. (Online)*, **9** (LLNL-JRNL-736881).

Good, P., T. Andrews, R. Chadwick, J.L. Dufresne, J.M. Gregory, J.A. Lowe, N. Schaller, and H. Shiogama, 2016: NonlinMIP contribution to CMIP6: model intercomparison project for non-linear mechanisms: physical basis, experimental design and analysis principles (v1. 0). *Geosci. Model Dev.*, **9(11)**, 4019-4028.

Gregory, J.M., W.J. Ingram, M.A. Palmer, G.S. Jones, P.A. Stott, R.B. Thorpe, J.A. Lowe, T.C. Johns, and K.D. Williams, 2004: A new method for diagnosing radiative forcing and climate sensitivity. *Geophys. Res. Lett.*, **31(3)**, L03205, doi:10.1029/2003GL018747.

Kravitz, B., A. Robock, O. Boucher, H. Schmidt, K.E. Taylor, G. Stenchikov, and M. Schulz, 2011: The Geoengineering Model Intercomparison Project (GeoMIP). *Atmos. Sci. Lett.*, **12**, 162-167, DOI:10.1002/asl.316.

Lewis N., and J.A. Curry, 2011: The implications for climate sensitivity of AR5 forcing and heat uptake estimates. *Clim. Dynam.*, **45(3-4)**, 1009-1023.

Marsh, D.R., J.F. Lamarque, A.J. Conley, and L.M. Polvani, 2016: Stratospheric ozone

chemistry feedbacks are not critical for the determination of climate sensitivity in CGeophysACCM). *Geophys. Res. Lett.*, **43(8)**, 3928-3934.

Montgomery, D.C., E.A. Peck, and G.G. Vining, 2012: *Introduction to linear regression analysis*. Fifth Edition, John Wiley and Sons. 672pp.

Muthers, S., J.G. Anet, A. Stenke, C.C. Raible, E. Rozanov, S. Brönnimann, T. Peter, F.X. Arfeuille, A.I. Shapiro, J. Beer, F. Steinhilber, Y. Brugnara, and W. Schmutz, 2014: The coupled atmosphere-chemistry-ocean model SOCOL-MPIOM, *Geosci. Model Dev.*, **7**, 2157-2179, https://doi.org/10.5194/gmd-7-2157-2014.

Natio, Y. and S. Yoden, 2005: A statistical analysis on the effects of the equatorial QBO on the extratropical stratosphere and troposphere based on large samples of daily data. *SOLA*, **1**, 17-20, https://doi.org/10.2151/sola.2005-007.

Noda, S., K. Kodera, Y. Adachi, M. Deushi, A. Kitoh, R. Mizuta, S. Murakami, K. Yoshida, and S. Yoden, 2017: Impact of interactive chemistry of stratospheric ozone on Southern Hemisphere paleoclimate simulation. *J. Geophys. Res.: Atmospheres*, **122(2)**, 878-895.

Noda, S., K. Kodera, Y. Adachi, M. Deushi, A. Kitoh, R. Mizuta, S. Murakami, K. Yoshida, and S. Yoden, 2018: Mitigation of global cooling by stratospheric chemistry feedbacks in a simulation of the Last Glacial Maximum. *J. Geophy. Res.: Atmospheres*, **123(17)**, 9378-9390.

Nowack, P.J., N.L. Abraham, P. Braesicke, and J.A. Pyle, 2018: The impact of stratospheric ozone feedbacks on climate sensitivity estimates. *J. Geophys. Res.:*

518 *Atmospheres*, **123**, https://doi.org/10.1002/2017JD027943.
519 Nowack, P.J., N.L. Abraham, A.C. Maycock, P. Braesicke, J.M. Gregory, M.M. Joshi, A.
520 Osprey, and J.A. Pyle, 2015: A large ozone-circulation feedback and its implications for
521 global warming assessments. *Nature Climate Change*, **5(1)**, 41-45.
522 Nowack, P.J., P. Braesicke, P., N.L. Abraham, and J.A. Pyle, 2017: On the role of ozone
523 feedback in the ENSO amplitude response under global warming. *Geophys. Res. Lett.*,
524 **44**, 3858-3866, doi:10.1002/2016GL072418.
525 Otto, A., F.E. Otto, O. Boucher, J. Church, G. Hegerl, P.M. Forster, N.P. Gillett, J. Gregory,
526 G.C. Johnson, R. Knutti, and N. Lewis, 2013: Energy budget constraints on climate
527 response. *Nature Geosci.*, **6(6)**, 415-416.
528 Skeie, R.B., T. Berntsen, M. Aldrin, M. Holden, and G. Myhre, 2014: A lower and more
529 constrained estimate of climate sensitivity using updated observations and detailed
530 radiative forcing time series. *Earth System Dynamics*, **5(1)**, 139-175.
531 Taylor, K.E., R.J. Stouffer, and G.A. Meehl, 2012: An overview of CMIP5 and the
532 experiment design. *Bull. Amer. Meteor. Soc.*, **93**, 485-498.
533 Yukimoto, S., Y. Adachi, M. Hosaka, T. Sakami, H. Yoshimura, M. Hirabara, T.Y. Tanaka, E.
534 Shindo, H. Tsujino, M. Deushi, and R. Mizuta, 2012: A new global climate model of the
535 Meteorological Research Institute: MRI-CGCM3—model description and basic
536 performance—. *J. Meteor. Soc. Japan*, **90**, 23-64, doi:10.2151/jmsj.2012-A02.
537 Yukimoto, S., H. Yoshimura, M. Hosaka, T. Sakami, H. Tsujino, M. Hirabara, T.Y. Tanaka,

M. Deushi, A. Obata, H. Nakano, Y. Adachi, E. Shindo, S. Yabu, T. Ose, and A. Kitoh, 2011: Meteorological Research Institute Earth System Model Version 1 (MRI-ESM1)—Model description. *Tech. Rep. Meteorol. Res. Inst.*, **64**, 83pp., Meteorol. Res. Inst., Tsukuba, Japan. 2011.

List of Figures

Fig. 1 (a) Time series of global and annual mean surface air temperature anomaly, ΔT_x (t), for ACTIVE (blue) and FIXED (red) simulations. (b) Net radiative flux (all components) at the TOA, ΔN_x (t), versus ΔT_x (t) for each year for ACTIVE (blue dots) and FIXED (red dots) simulations. Corresponding lines represent ordinary least squares regression fits to the last 100 years data. Dotted lines parallel to abscissa correspond to the time mean of ΔN_x (t) for the last 50 years.

Fig. 2 Graphical representation of the impact of ACTIVE simulation compared to FIXED one on ECS, climate forcing and climate feedbacks for MRI models, as denoted by a black dot. The abscissa R_α shows the ratio of the feedback parameter, whereas the ordinate R_F shows the ratio of the difference between the net radiation flux at the TOA and the imposed forcing. The red and blue dashed lines correspond to the % changes in ECS. Thick black dashed line shows the no-impact line and represents no impact on global warming ($R_F = R_\alpha$; Case 0). The region above the no-impact line corresponds to amplification of global climate change ($R_F > R_\alpha$; Case I for global warming, or Case II for global cooling), whereas the region below the no-impact line corresponds to reduction of global climate change ($R_F < R_\alpha$; Case III for global warming, or Case IV for global cooling). Solid black error bars show the uncertainties in R_α and R_F. The unity value of R_α represents no change in the climate feedback parameter α_x, and every 0.1 increase (or decrease) in the magnitude of

562 R_α corresponds to the 10% increase (or decrease) in feedback strength in ACTIVE as
563 compared to FIXED simulation. Similarly, unity value of R_F represents no change and
564 every ±0.1 increase in R_F represents ±10% change in difference of radiative flux
565 imbalance and forcing.
566
567 Fig. 3 (a) Same as Fig. 1 (b) but for clear-sky (CS) long-wave (LW) and short-wave (SW)
568 components for ACTIVE and FIXED simulations for 100 years. (b) Same as (a) but for
569 cloud-radiative effect (CRE). (c) Impact assessment on R_α - R_F plane for individual and
570 all-radiative components.
571
572 Fig. 4 Intercomparison of CMIP5 models for abrupt 4×CO_2 experiment relative to the multi-
573 model mean (MMM; $R_F = R_\alpha = 1$). Each model is plotted with its own symbol with standard
574 errors in R_F - R_α plane. See the main text for details.

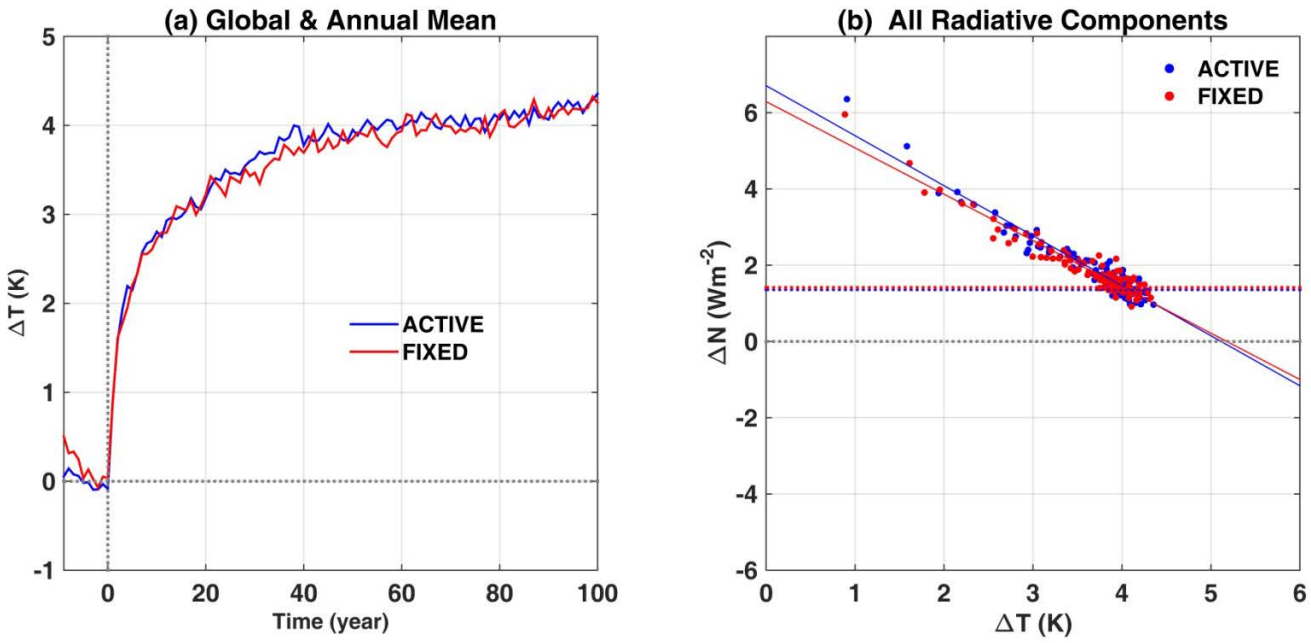

575 Fig. 1 (a) Time series of global and annual mean surface air temperature anomaly, ΔT_x
576 (t), for ACTIVE (blue) and FIXED (red) simulations. (b) Net radiative flux (all components)
577 at the TOA, ΔN_x (t), versus ΔT_x (t) for each year for ACTIVE (blue dots) and FIXED (red
578 dots) simulations. Corresponding lines represent ordinary least squares regression fits to
579 the last 100 years data. Dotted lines parallel to abscissa correspond to the time mean of
580 ΔN_x (t) for the last 50 years.

581 .

582

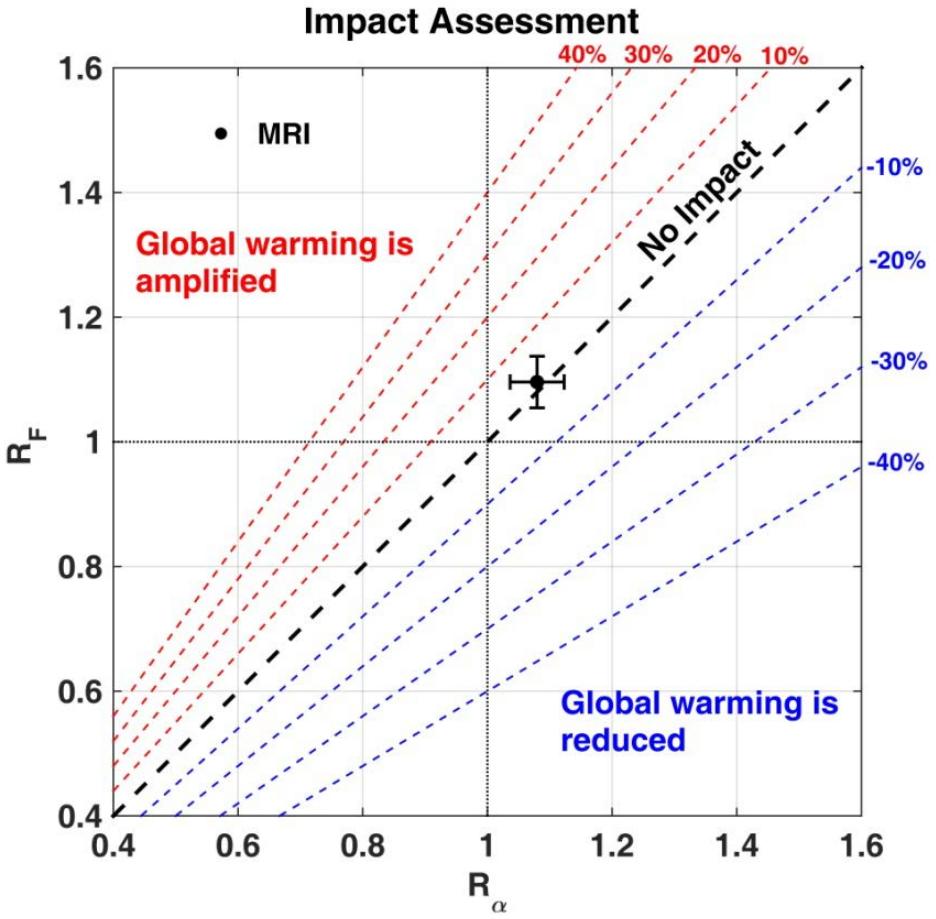

583

584 Fig. 2 Graphical representation of the impact of ACTIVE simulation compared to FIXED
585 one on ECS, climate forcing and climate feedbacks for MRI models, as denoted by a black
586 dot. The abscissa R_α shows the ratio of the feedback parameter, whereas the ordinate R_F
587 shows the ratio of the difference between the net radiation flux at the TOA and the imposed
588 forcing. The red and blue dashed lines correspond to the % changes in ECS. Thick black
589 dashed line shows the no-impact line and represents no impact on global warming (R_F =
590 R_α; Case 0). The region above the no-impact line corresponds to amplification of global
591 climate change ($R_F > R_\alpha$; Case I for global warming, or Case II for global cooling), whereas
592 the region below the no-impact line corresponds to reduction of global climate change (R_F

593 < R_α ; Case III for global warming, or Case IV for global cooling). Solid black error bars
594 show the uncertainties in R_α and R_F. The unity value of R_α represents no change in the
595 climate feedback parameter α_x, and every 0.1 increase (or decrease) in the magnitude of
596 R_α corresponds to the 10% increase (or decrease) in feedback strength in ACTIVE as
597 compared to FIXED simulation. Similarly, unity value of R_F represents no change and
598 every ±0.1 increase in R_F represents ±10% change in difference of radiative flux
599 imbalance and forcing.
600

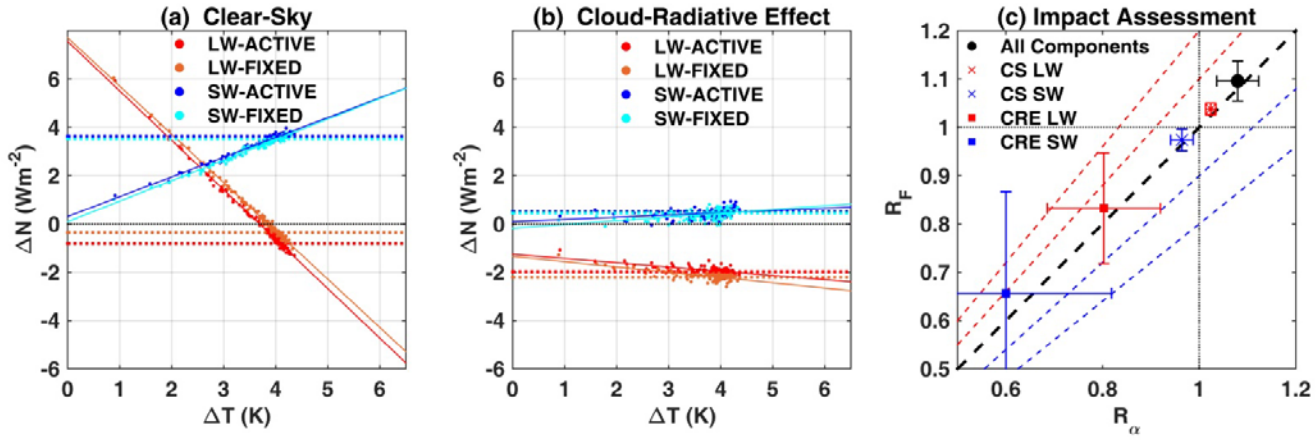

601 Fig. 3 (a) Same as Fig. 1 (b) but for clear-sky (CS) long-wave (LW) and short-wave (SW)
602 components for ACTIVE and FIXED simulations for 100 years. (b) Same as (a) but for
603 cloud-radiative effect (CRE). (c) Impact assessment on R_α - R_F plane for individual and
604 all-radiative components.

605

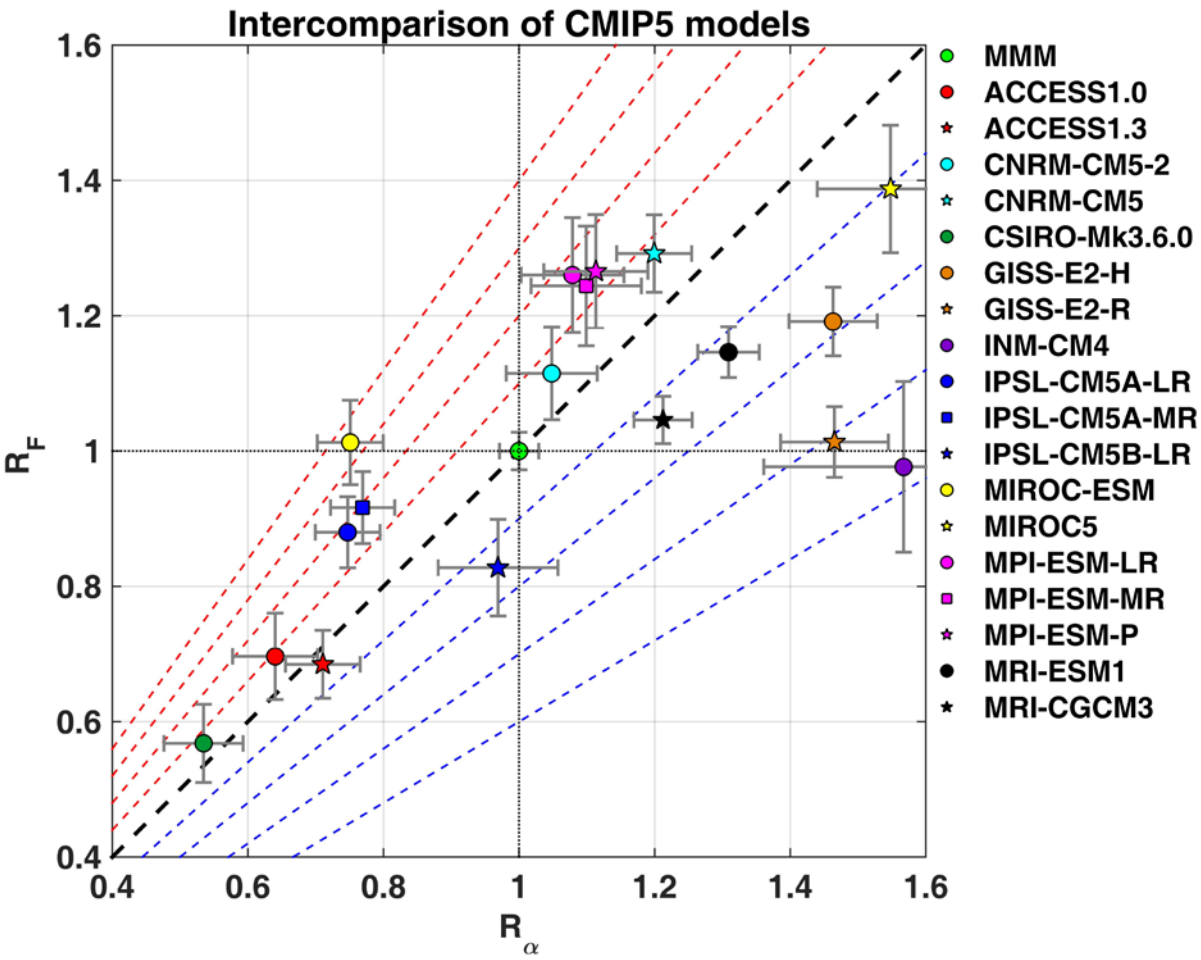

606 Fig. 4 Intercomparison of CMIP5 models for abrupt 4×CO_2 experiment relative to the multi-

607 model mean (MMM; $R_F = R_\alpha = 1$). Each model is plotted with its own symbol with standard

608 errors in R_F - R_α plane. See the main text for details.

609

List of Tables

Table 1 Summary of the parameters obtained from the linear regression fits and uncertainty in their estimation.

	All radiation	**CS LW**	**CS SW**	**CRE LW**	**CRE SW**
$\alpha_{ACTIVE} \pm E_{\alpha,ACTIVE}$	-1.312 ± 0.037	-2.048 ± 0.016	0.819 ± 0.014	-0.175 ± 0.019	0.093 ± 0.029
$\alpha_{FIXED} \pm E_{\alpha,FIXED}$	-1.215 ± 0.035	-2.000 ± 0.014	0.850 ± 0.014	-0.218 ± 0.021	0.154 ± 0.029
$F_{ACTIVE} \pm E_{F,ACTIVE}$	6.708 ± 0.137	7.561 ± 0.060	0.309 ± 0.054	-1.256 ± 0.073	0.094 ± 0.108
$F_{FIXED} \pm E_{F,FIXED}$	6.290 ± 0.129	7.714 ± 0.052	0.094 ± 0.052	-1.345 ± 0.076	-0.173 ± 0.105
$\overline{\Delta N}_{ACTIVE} \pm E_{N,ACTIVE}$	1.363 ± 0.031	-0.813 ± 0.034	3.645 ± 0.016	-1.975 ± 0.017	0.506 ± 0.024
$\overline{\Delta N}_{FIXED} \pm E_{N,FIXED}$	1.413 ± 0.032	-0.352 ± 0.038	3.519 ± 0.018	-2.208 ± 0.018	0.454 ± 0.027
$R_{\alpha} \pm E_{R\alpha}$	1.080 ± 0.043	1.024 ± 0.011	0.964 ± 0.023	0.803 ± 0.117	0.600 ± 0.219
$R_F \pm E_{RF}$	1.096 ± 0.041	1.038 ± 0.012	0.974 ± 0.023	0.833 ± 0.115	0.657 ± 0.210
% change in ECS $\pm$ δ**ECS (%)**	1.502 ± 5.597	1.391 ± 1.574	1.015 ± 3.381	3.737 ± 20.806	9.404 ± 53.048

615 Table 2 Summary of parameters obtained for CMIP5 models for abrupt 4×CO2 experiment.

616

	$\alpha \pm E_\alpha$	$F \pm E_F$	$\overline{\Delta N} \pm E_N$	$R_\alpha \pm E_{R\alpha}$	$R_F \pm E_{RF}$	% change in ECS $\pm \delta ECS$ (%)
MMM	-1.002 ± 0.020	6.542 ± 0.090	1.878 ± 0.017	1.000 ± 0.029	1.000 ± 0.028	-
ACCESS1.0	-0.641 ± 0.062	5.273 ± 0.287	2.024 ± 0.043	0.640 ± 0.063	0.697 ± 0.064	8.811± 14.602
ACCESS1.3	-0.712 ± 0.053	5.259 ± 0.223	2.066 ± 0.032	0.711 ± 0.055	0.685 ± 0.050	-3.621± 10.291
CNRM-CM5-2	-1.050 ± 0.064	7.260 ± 0.301	2.062 ± 0.029	1.048 ± 0.067	1.115 ± 0.068	6.345± 9.436
CNRM-CM5	-1.202 ± 0.050	7.738 ± 0.238	1.713 ± 0.030	1.199 ± 0.055	1.292 ± 0.057	7.723± 6.893
CSIRO-Mk3.6.0	-0.536 ± 0.057	4.638 ± 0.259	1.990 ± 0.054	0.535 ± 0.058	0.568 ± 0.058	6.231± 15.860
GISS-E2-H	-1.466 ± 0.058	7.115 ± 0.208	1.559 ± 0.028	1.463 ± 0.065	1.191± 0.051	-18.580 ± 5.017
GISS-E2-R	-1.468 ± 0.074	6.518 ± 0.224	1.792 ± 0.027	1.465 ± 0.080	1.013 ± 0.052	-30.841± 5.179
INMCM4	-1.570 ± 0.204	6.292 ± 0.581	1.738 ± 0.027	1.567 ± 0.206	0.977 ± 0.126	-37.687± 11.487
IPSL-CM5A-LR	-0.749 ± 0.045	6.137 ± 0.229	2.034 ± 0.034	0.747 ± 0.048	0.880 ± 0.053	17.770 ± 10.304
IPSL-CM5A-MR	-0.771 ± 0.045	6.408 ± 0.232	2.134 ± 0.028	0.769 ± 0.047	0.916 ± 0.053	19.125 ± 10.084
IPSL-CM5B-LR	-0.971 ± 0.086	5.087 ± 0.319	1.227 ± 0.055	0.969 ± 0.088	0.828 ± 0.071	-14.597 ± 10.716
MIROC-ESM	-0.753 ± 0.046	7.575 ± 0.274	2.852 ± 0.034	0.751 ± 0.049	1.013 ± 0.062	34.833 ± 12.051
MIROC5	-1.551 ± 0.104	8.511 ± 0.416	2.041 ± 0.060	1.548 ± 0.108	1.387 ± 0.094	-10.373 ± 8.732
MPI-ESM-LR	-1.081 ± 0.073	7.874 ± 0.375	1.997 ± 0.051	1.079 ± 0.076	1.260 ± 0.085	16.807 ± 11.376
MPI-ESM-MR	-1.101 ± 0.078	7.665 ± 0.392	1.864 ± 0.058	1.099 ± 0.081	1.244 ± 0.088	13.195 ± 11.615
MPI-ESM-P	-1.115 ± 0.074	7.843 ± 0.370	1.942 ± 0.059	1.113 ± 0.077	1.265 ± 0.084	13.674 ± 10.892
MRI-ESM1	-1.312 ± 0.037	6.708 ± 0.137	1.363 ± 0.031	1.309 ± 0.045	1.146 ± 0.038	-12.441 ± 4.169
MRI-CGCM3	-1.215 ± 0.035	6.290 ± 0.129	1.413 ± 0.032	1.212 ± 0.043	1.046 ± 0.035	-13.736 ± 4.204

617